Self-assembly of highly luminescent bi-1,3,4-oxadiazole derivatives through electron donor–acceptor interactions in three-dimensional crystals, two-dimensional layers and mesophases†

Songnan Qu,[a] Xiaofang Chen,[b] Xiang Shao,[b] Fan Li,[a] Hongyu Zhang,[c] Haitao Wang,[a] Peng Zhang,[a] Zhixin Yu,[a] Kai Wu,[b] Yue Wang[c] and Min Li*[a]

Received 11th March 2008, Accepted 3rd June 2008
First published as an Advance Article on the web 9th July 2008
DOI: 10.1039/b804189j

We report on the synthesis and self-assembly of a new series of highly luminescent bi-1,3,4-oxadiazole derivatives [2,2′-bis(4-alkoyphenyl)-bi-1,3,4-oxadiazole, BOXD-*n*, $n = 1, 3, 4, 5, 6, 7, 10, 16$]. Fully conjugated conformations were demonstrated either by computer simulation or in a single-crystal state. Well-defined 3D donor–acceptor (DA) architectures with strong face-to-face and edge-to-edge donor–acceptor interactions were observed in the single-crystal structure of BOXD-1. Highly oriented face-on two-dimensional DA layered structures due to edge-to-edge donor–acceptor interactions were observed on highly oriented pyrolytic graphite (HOPG) in BOXD-7 and BOXD-16. Nematic phase, smectic C phase with large tilted angle ($\theta \approx 50°$) and relatively large transition enthalpic values and a highly ordered smectic X phase were demonstrated in BOXD-*n* ($n = 5, 6, 7, 8, 10, 16$) through tailing the terminal chains and relatively large scale monodomains were prepared in the smectic X phase of BOXD-5 even without any surface treatment. Strong blue fluorescent emissions were observed in BOXD-6 either in cyclohexane ($\Phi_F \approx 92\%$) or in solid state ($\Phi_F \approx 57\%$). The donor–acceptor interactions between alkyoxyphenylene rings and 1,3,4-oxadiazole rings were thought to be the driving force for the molecules to self-assemble into a large angle tilted layered structure.

Introduction

Self-assembly of molecules through noncovalent interactions into various superstructures opens new possibilities of constructing novel materials in biology and materials fields.[1] Among the noncovalent interactions, electron donor–acceptor (DA) interactions have attracted great attention, and have been applied in many areas, such as in crystal engineering,[2] molecular recognition[3] and organic electronics.[4] Especially, aromatic molecules with well-defined DA architectures are considered to be promising materials for actual implementation in high-efficiency devices.

Liquid crystalline materials, which present self-organizing ability, fluidity, and easy defect-free orientation with special treatment, have been recently recognized to have great advantages in manipulation of optimized high-efficiency organic electro-optic devices.[5] Meanwhile, works on liquid crystals have demonstrated that electron transfer between electron donors and acceptors in liquid crystals has a profound effect on the induction and stabilization of the mesophases.[6] Such kinds of liquid crystalline complexes can be prepared either by doping pure liquid crystalline phases with acceptor (or donor) molecules or from covalently linked donor–acceptor mesogens. Mixtures containing triphenylene as the donor and trinitrofluorenone,[7] azatriphenylenes[8] and mellitic trimides[9] as acceptors, have been investigated and the results showed that alternating stacking of the donor and acceptor in equimolar mixtures could enhance the columnar stability, and lead to considerably higher mobilities.[10] Formation of columnar mesophases from covalently linked donor–acceptor mesogens has been studied, in particular, by Janietz,[11] who synthesized, *e.g.*, complexes of electron-rich pentaalkynylbenzene attached directly to trinitrofluorenone (TNF).[12] In these systems, strong intermolecular electron donor–acceptor interactions lead to the formation of highly ordered columnar mesophases.

1,3,4-Oxadiazole derivatives have enjoyed widespread use as electron-transporting/hole blocking (ECHB) materials, emitting layers in electroluminescent diodes and non-linear optical materials, due to the electron-deficient nature of the heterocycle, high photoluminescence quantum yield and good thermal and chemical stabilities of the materials.[13] Investigations on 1,3,4-oxadiazole derivatives (OXDs) in crystals showed that electron donor (phenylene rings)–acceptor (1,3,4-oxadiazole rings) interaction is responsible for the stacking of molecules of some of the oxadiazole derivatives in their crystalline states.[14] Different

[a]*Key Laboratory of Automobile Materials (Jilin University), Ministry of Education, Institute of Materials Science and Engineering, Jilin University, Changchun 130012, P. R. China. E-mail: minli@jlu.edu.cn; Tel: +86 431 5168254*
[b]*Beijing National Laboratory for Molecular Sciences, College of Chemistry and Molecular Engineering, Peking University, Beijing 100871, P. R. China. E-mail: chenxiaofang@pku.edu.cn; Fax: +86 10 62754187*
[c]*Key Laboratory for Supramolecular Structure and Materials of Ministry of Education, College of Chemistry, Jilin University, Changchun 130012, P. R. China. E-mail: yuewang@jlu.edu.cn; Fax: +86 431 5193421*

† Electronic supplementary information (ESI) available: DSC charts and X-ray diffraction patterns of BOXD-*n* ($n = 5, 6, 7, 8, 10, 16$), computational details and crystal data for BOXD-1. CCDC reference number for BOXD-1 CCDC 293679. For ESI and crystallographic data in CIF or other electronic format see DOI: 10.1039/b804189j

types of liquid crystalline 1,3,4-oxadiazole derivatives have been reported in the literature. Columnar mesophases were formed in star-shaped[15] and discotic OXDs,[16] while for rod shaped OXDs, Tokuhisa *et al.* reported that the charge mobility is one order of magnitude higher in the higher ordered SmX phase (1×10^{-3} cm^2 V^{-1} s^{-1}) than that in SmA phase.[17] Meanwhile, it should be noted that extensive investigation on the effect of charge transfer interaction on the self-assembly behavior of OXDs in mesophases is relatively rare. Recently, we reported the synthesis and mesomorphic properties of a new series of twin-taped bi-1,3,4-oxadiazole derivatives [2,2′-bis(3,4,5-trialkoxyphenyl)-bi-1,3,4-oxadiazole, BOXD-T*n*, $n = 3, 4, 5, 6, 7, 8, 10, 14$].[18] They have been confirmed to give rise to columnar mesophases and exhibit strong blue fluorescent emissions either in cyclohexane or in bulk. Our present work is aimed at developing a new series of 1,3,4-oxadiazole derivatives, using electron donor–acceptor interactions to enhance the stability and packing order in the solid states and mesophases. The newly designed molecules, namely, [2,2′-bis(4-alkoyphenyl)-bi-1,3,4-oxadiazole, BOXD-*n*, $n = 1, 3, 4, 5, 6, 7, 8, 10, 16$], can be regarded as D–A–A–D molecules. The novelty of the present work is that well-defined 3D DA architectures due to the presence of both strong face-to-face and edge-to-edge donor–acceptor interactions were obtained in a single-crystal structure of BOXD-1; highly oriented face-on two-dimensional DA layered structures due to edge-to-edge donor–acceptor interactions were observed on highly oriented pyrolytic graphite (HOPG) in BOXD-7 and BOXD-16; nematic phase, SmC phase with a large tilt angle ($\theta \approx 50°$) and relatively large transition enthalpic values, and a highly ordered SmX phase were demonstrated in BOXD-*n* ($n = 5, 6, 7, 8, 10, 16$) through tailing the terminal chains; and relatively large scale monodomains were prepared in the SmX phase of BOXD-5 even without any surface treatment; strong blue fluorescent emissions were observed in BOXD-6 either in cyclohexane ($\Phi_F \approx 92\%$) or in solid state ($\Phi_F \approx 57\%$). The driving force for the peculiar self-assembly behavior of BOXD-*n* is also discussed.

Results and discussion

Synthesis

Scheme 1 shows the synthetic route for BOXD-*n*. The bi-dihydrazine derivatives **3** were prepared by the route reported in our previous work.[19] The purified **3** was dissolved in phosphorous oxychloride ($POCl_3$) and refluxed for about 40 h. Excess $POCl_3$ was removed through distillation and the residue was slowly added to the ice-water. After removal of the solvent under reduced pressure, the final product BOXD-*n* was purified by recrystallization from DMSO for further NMR, FT-IR spectroscopy and elemental analysis.

Molecular conformation

It is well known that the molecular conformation influences the optical and electronic properties of molecules as well as the molecular assembly behaviors. To study the conformation of BOXD-*n*, the geometry of BOXD-*n* ($n = 1, 5, 6, 7, 8, 10, 16$) has been optimized within the generalized gradient approximation (GGA) associated with the PW91 functional for correlation and 'DNP' basis set. The linear coplanar conformations of BOXD-*n*

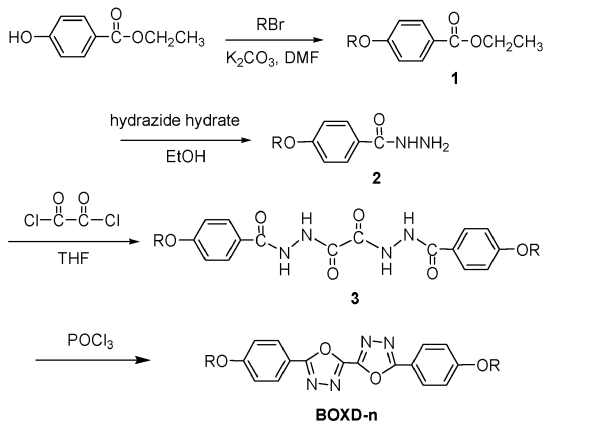

BOXD-1: R= $-CH_3$ **BOXD-3**: R= $-(CH_2)_2CH_3$ **BOXD-4**: R= $-(CH_2)_3CH_3$
BOXD-5: R= $-(CH_2)_4CH_3$ **BOXD-6**: R= $-(CH_2)_5CH_3$ **BOXD-7**: R= $-(CH_2)_6CH_3$
BOXD-8: R= $-(CH_2)_7CH_3$ **BOXD-10**: R= $-(CH_2)_9CH_3$ **BOXD-16**: R= $-(CH_2)_{15}CH_3$

Scheme 1 Synthesis of BOXD-*n*.

($n = 1, 5, 6, 7, 8, 10, 16$) were confirmed to exhibit the lowest energy. The phenyl rings and oxadiazole rings of BOXD-*n* are coplanar and the bond lengths of phenyl–oxadiazole and oxadiazole–oxadiazole are 1.43 Å and 1.44 Å, respectively, indicating that the rigid backbone of BOXD-*n* molecules is nearly coplanar and fully conjugated.

X-Ray single-crystal analysis on BOXD-1

Suitable crystals of BOXD-1 were grown at room temperature from chloroform by slow evaporation of the solvent. Crystal data are given in the ESI. The molecular structure of BOXD-1 in the single-crystal state is shown in Fig. 1. The molecular geometry of BOXD-1 is centrosymmetric. The torsion angles of the phenyl ring to the oxadiazole ring and the oxadiazole ring to the oxadiazole ring are 0.55° and 0.16° respectively. The bond lengths of phenyl–oxadiazole and oxadiazole–oxadiazole are 1.45 Å which corresponds well to the range for a C(sp2) – C(sp2) single bond (1.48 Å).[20] This indicates that the four rings of BOXD-1 molecules in the single-crystal are coplanar and thus fully conjugated, which is similar to that calculated above. The BOXD-1 molecules formed a layered structure that consists of infinite stacks as seen from the view of the *c*-direction (Fig. 2b, c). Molecules are large angle tilted against the *b*-direction (about 53°) in the same layer, and the orientations of molecules in adjacent layers made an angle of about 34° and kept the same in odd or even layers. Molecules are arranged parallel to form slipped stacks, within which the short axis of the molecular plane is inclined about 44° against the stack axis (Fig. 2c). The

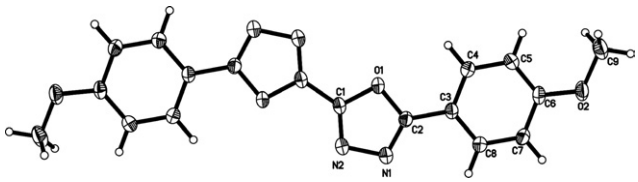

Fig. 1 Molecular structure of BOXD-1 in a single-crystal. Thermal ellipsoids enclose 50% of the electron density.

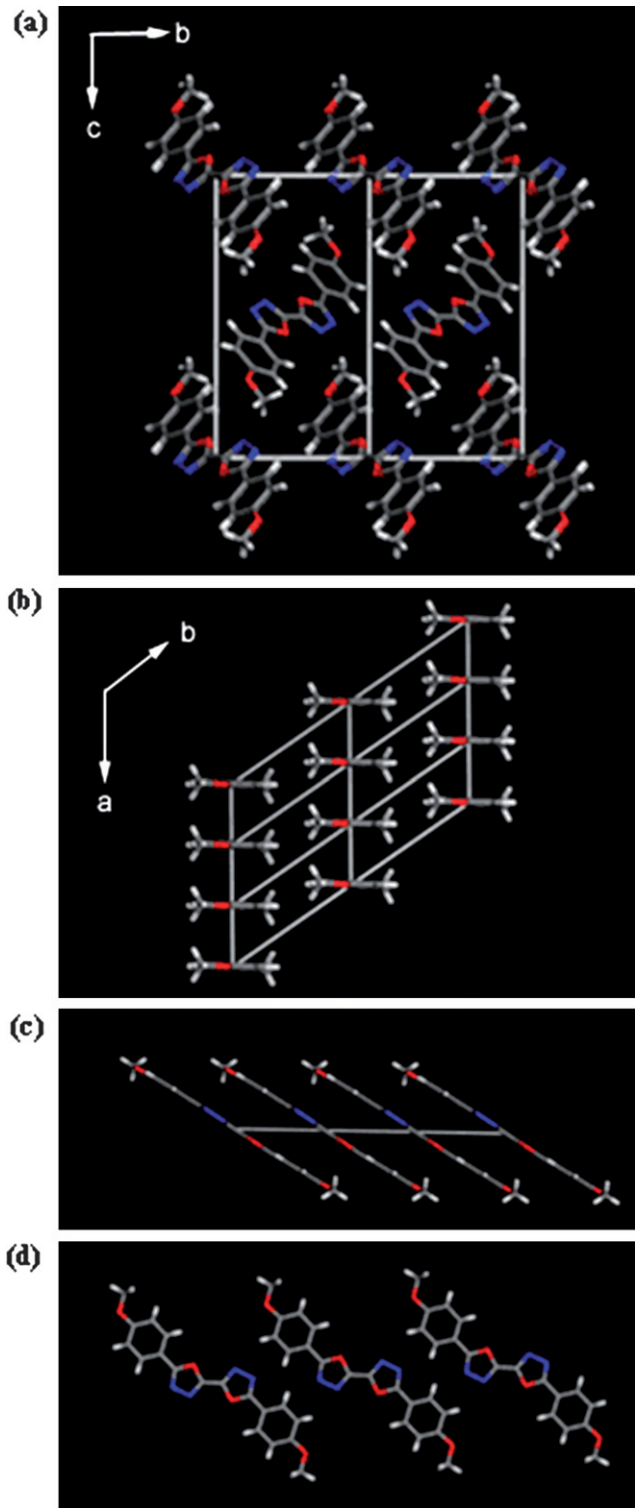

Fig. 2 Molecular packing of BOXD-1 in a single-crystal state (a) viewed along the *a*-axis, (b) viewed in the *a*,*b* plane without the *c*-axis, (c) viewed in the *a* direction, (d) viewed in the (*a* + *b*) direction.

orientation of molecules is the same in different stacks within the same layer. The 1,3,4-oxadiazole rings (π-acceptor) of one molecule are located between the phenyl rings (π-donor) of neighboring molecules in a stack, and thus form an alternating AD architecture along the *a*-axis. The distance between the molecular planes amounts to 3.28 Å, which is short enough to give rise to face-to-face donor–acceptor interactions and induces the formation of π-complexes. The estimated face-to-face interactions between one pair of BOXD-1 molecules in stacks are around 15.2 kJ mol^{-1}. The AD architecture can also be found along the (*a* + *b*) direction in which the oxadiazole rings in one stack are close to the phenyl rings in the neighborind stacks [closest H (phenyl ring)–N (oxadiazole ring) distance: 2.81 Å] (Fig. 2d), and the edge-to-edge interactions between one pair of BOXD-1 molecules in the (*a* + *b*) direction was estimated to be around 14.7 kJ mol^{-1}. It is clear that both face-to-face and edge-to-edge donor–acceptor interactions between BOXD-1 molecules are responsible for the formation of well-defined 3D DA architectures.

Two-dimensional assembling behavior

With the development in preparing supramolecular assemblies and molecular nanostructures, the precise control of the structure of two-dimensional (2D) molecular assemblies attracts increasing attention.[21] The well-established scanning tunneling microscopy (STM) technique has been successfully used to study the structure of self-assembled monolayers (SAMs) and their ordering, molecular orientation, intermolecular reaction, and structural transformation,[22] which are important from the viewpoint of applying these materials in thin-film devices. The self-assembling behaviors of BOXD-7 and BOXD-16 on highly oriented pyrolytic graphite (HOPG) were investigated by STM. The adlayer was prepared by directly depositing a droplet of the phenyloctane solution of BOXD-*n* onto the HOPG surface.

BOXD-7 and BOXD-16 molecules spontaneously adsorb on the HOPG surface and self-organize into a two-dimensional (2D) assembly with a well-defined structure. Large scale domains (100 nm × 100 nm) without structural defects were observed for BOXD-7 on HOPG, as shown in Fig. 3a. The STM image reveals the ordered nanosegregated structure of the BOXD-7 molecules with remarkably alternating bright bands and dark stripes over the whole scanning area. Owing to the large electronic density of aromatic rings, the aromatic part of the molecule appears brighter in contrast to that of the alkyl chains.[23] Thus, it is reasonable to attribute the bright bands to the aromatic parts of molecules and the darker ones to the alkyl chains. As shown in Fig. 3b, the phenyl rings appear as bright spots, while the oxadiazole rings are relatively dark and are not well resolved. The widths of the bright and dark bands are measured to be 1.5 ± 0.2 nm and 1.1 ± 0.2 nm, respectively. Due to the low resolution of this image, we were not able to give the subtle details of the BOXD-7 molecules on HOPG. However, high-resolution STM images of BOXD-16 on HOPG are obtained (Fig. 4a). The width of the dark band corresponding to the alkyl chains of BOXD-16 molecules is measured to be 2.4 ± 0.2 nm. The length of one alkyl side chain of a BOXD-16 molecule is measured to be 2.0 ± 0.2 nm, corresponding to the length of one cetyloxyl chain and indicating that the alkyl chains of BOXD-16 molecules are tilted against the layer normal with an angle of 56° ± 2°. In consideration of the fact that the ratio of the dark band width to the alkyl chain length of BOXD-16 is similar to that of BOXD-7, it is reasonable to assume that the alkyl chains of BOXD-7 are tilted against the layer normal with the same angle as that of

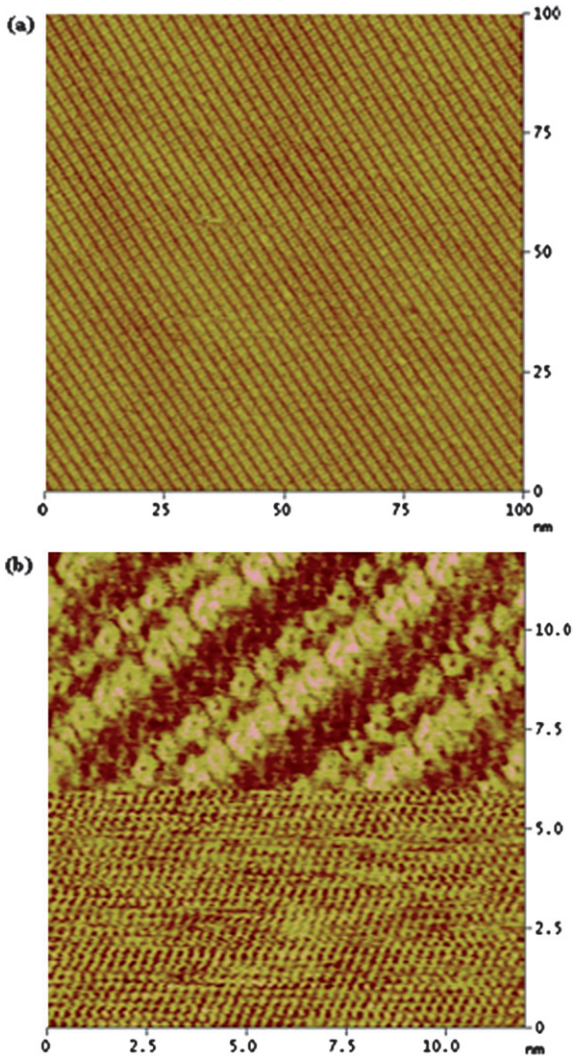

Fig. 3 (a) A large scale STM image of BOXD-7 self-assembly on a HOPG surface (recorded with $V = -1000$ mV, $I = 98$ pA). (b) A hybrid STM image showing the orientations of the BOXD-7 adlayer and the underlying HOPG lattice. The imaging voltage was 800 mV for the upper part and then suddenly changed to 50 mV during the scanning to image the underlying substrate lattice, while the tunneling current was kept at 250 pA.

BOXD-16. Interestingly, the widths of the bright bands in the STM images of both BOXD-7 and BOXD-16 are the same (1.5 ± 0.2 nm), which are shorter than the calculated length of their rigid core (about 1.7 nm), suggesting that they are tilted to the layer normal. It can therefore be concluded that both BOXD-7 and BOXD-16 show the same aggregating behavior on the HOPG surface. From the structural information in the STM image, a molecular model is superimposed in Fig. 4a. The high-resolution image reveals that the alkyl chains of BOXD-16 in the adjacent lamellae all adopt a tail-to-tail packing geometry. BOXD-16 molecules are orderly arranged on HOPG to form highly oriented two-dimensional molecular layers in which the linearly coplanar molecules *syn*-incline (about $51° \pm 2°$) to the layer normal. The proposed molecular arrangement model and a unit cell of BOXD-16 assembly according to the STM observations are depicted in Fig. 4c. The unit cell parameters are $a = 0.9 \pm 0.2$ nm, $b = 6.0 \pm 0.2$ nm, and $\alpha = 38 \pm 2°$. It can be seen that the molecule's are large angle tilted in the adlayer and thus, the oxadiazole rings of one molecule and the phenyl rings of its neighboring molecules are close to each other within the same layer. Such a packing mode will cause donor–acceptor interactions between adjacent molecules, which is similar to the packing motif observed along the [110] direction in a single-crystal of BOXD-1. The edge-to-edge donor–acceptor interactions between BOXD-7 and BOXD-16 molecules can account for the formation of highly oriented two-dimensional DA architectures on the HOPG surface.

To understand the orientation between molecular assembly and the underlying HOPG surface, we acquired a hybrid STM image. Fig. 4b presents a typical image where both the orientations of the BOXD-16 molecules and the underlying graphite lattice are simultaneously imaged. From the image, the α angle between the molecular long axis (direction b_1) and the substrate lattice direction a_1 is measured to be $120° \pm 2°$, indicating a definite crystal relationship between the molecules and the HOPG substrate. The β angle between direction c_1 and the substrate lattice direction a_1 was measured to be $22° \pm 2°$, indicating a mismatch between the adlayer and substrate symmetry. Thus, the edge-to-edge donor–acceptor interactions between the alkylphenylene rings and the 1,3,4-oxadiazole rings of the neighboring molecules could be the driving force for the formation of the slipped stacks of the BOXD-7 and BOXD-16 molecules on HOPG, while the stacks are regularly packed into the lamellar configuration through van der Waals interaction between the alkyl chains. It can be envisioned that the highly oriented two-dimensional DA architectures of BOXD-*n* might lead to some interesting optical or electrical properties, which is now in progress.

Mesomorphic properties of BOXD-*n*

The phase transition temperatures and transition enthalpies for BOXD-*n* ($n = 3, 4, 5, 6, 7, 8, 10, 16$) are summarized in Table 1. It can be seen that the mesophase behaviors are greatly affected by the length of the terminal chains. BOXD-3 and BOXD-4 are non-mesomorphic perhaps due to the short alkoxyl terminal groups which cause the higher melting point and thus suppress the LC phase. On the other hand, BOXD-*n* ($n = 5, 6, 7, 8, 10, 16$) with longer alkoxyl terminal groups showed enantiotropic LC behaviors as confirmed by POM, DSC and XRD investigations. A plot of the transition temperatures as a function of the length of the terminal *n*-alkyl chain for BOXD-*n* on the cooling runs is shown in Fig. 5. It is obvious that both the melting and isotropic temperatures of BOXD-*n* showed odd–even effect on going from $n = 3$ to 8 and the oscillation in the temperatures became weaker with the increase of *n*.

BOXD-*n* ($n = 5, 6, 7$) exhibited polymesomorphic phase sequences. On slowly cooling from the isotropic state of BOXD-6 sandwiched between untreated glass slides, birefringent droplets first appeared which vanished subsequently to give rise to large areas of homeotropic texture, which flashed when subjected to mechanical stress (Fig. 6a). Similar textures were observed for BOXD-5 on cooling from its isotropic phase. These are the characteristic features of the nematic phase. The powder X-ray diffraction of BOXD-6 at 180 °C (Fig. 7a) exhibited two diffuse

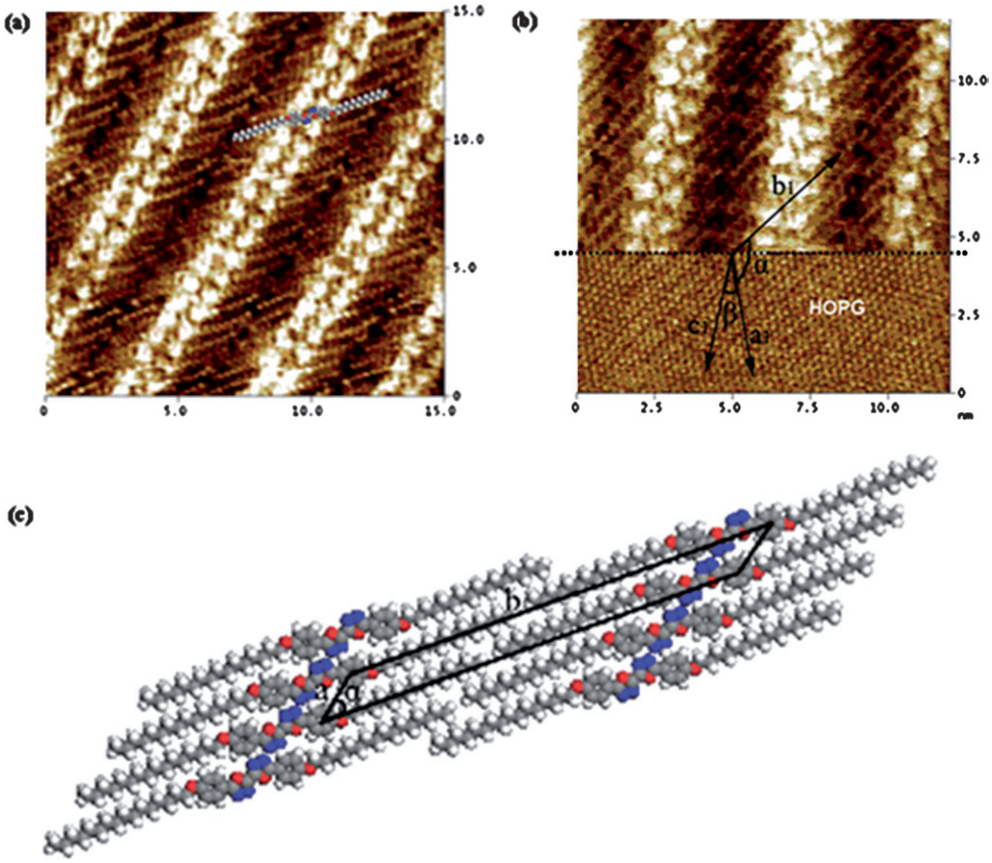

Fig. 4 (a) High-resolution STM image recorded at $V = 800$ mV and $I = 500$ pA. (b) A bybrid STM image showing the orientations of the BOXD-16 adlayer and the underlying HOPG lattice. During the scanning from top to bottom, the bias voltage was suddenly changed to 50 mV from 800 mV while the tunneling current was kept unchanged at 400 pA. In such a way, the underlying HOPG lattice and the molecular adlayer could be simultaneously observed in a single image. (c) Structural model for the self-assembly.

peaks centered at *d*-spacings of 17.8 Å and 4.5 Å, respectively, strongly suggesting its nematic feature, which fits well with the POM observations. It should be noted that the enthalpic value for this nematic–isotropic transition of BOXD-*n* is in the range of 2.4 to 3.5 kJ mol^{-1}, which is larger than the conventional nematic–isotropic transition enthalpies (< 1 kJ mol^{-1}) of calamitic mesogens, indicating that relatively strong intermolecular interactions might exist in their nematic phases.

Table 1 Phase transition temperatures (T/°C) and enthalpies (ΔH/kJ mol^{-1} in brackets) of BOXD-*n* ($n = 3, 4, 5, 6, 7, 8, 10, 16$) determined by DSC at a scan rate of 10 °C min^{-1}

Compound	Heating		Cooling	
BOXD-3	Cr–I	224.1(36.5)	I–Cr	221.5(37.1)
BOXD-4	Cr–I	207.0(39.5)	I–Cr	204.0(38.9)
BOXD-5	Cr–SmX	147.1(8.9)	SmX–Cr	119.5(9.4)
	SmX–N	186.0(26.3)	N–SmX	183.3(25.7)
	N–I	187.9(2.4)	I–N	186.4(2.4)
BOXD-6	Cr_1–Cr_2	101.5(5.5)	SmX–Cr_1	164.7(10.0)
	Cr_2–Cr_3	145.5(6.8)	SmC–SmX	175.3(11.5)
	Cr_3–N	181.2(31.6)	N–SmC	177.7(8.7)
	N–I	190.0(3.5)	I–N	188.4(3.5)
BOXD-7			SmX–Cr	154.2(13.6)
	Cr–SmC	174.7(27.8)	SmC–SmX	164.9(13.2)
	SmC–I	185.0(17.3)	I–SmC	182.2(17.1)
BOXD-8	Cr–SmC	165.0(28.7)	SmC–Cr	156.2(28.8)
	SmC–I	187.6(19.2)	I–SmC	185.9(18.2)
BOXD-10	Cr–SmC	149.5(38.4)	SmC–Cr	144.9(38.1)
	SmC–I	187.3(19.3)	I–SmC	187.1(19.2)
BOXD-16	Cr–SmC	139.7(47.5)	SmC–Cr	135.8(48.9)
	SmC–I	175.0(19.2)	I–SmC	174.3(18.8)

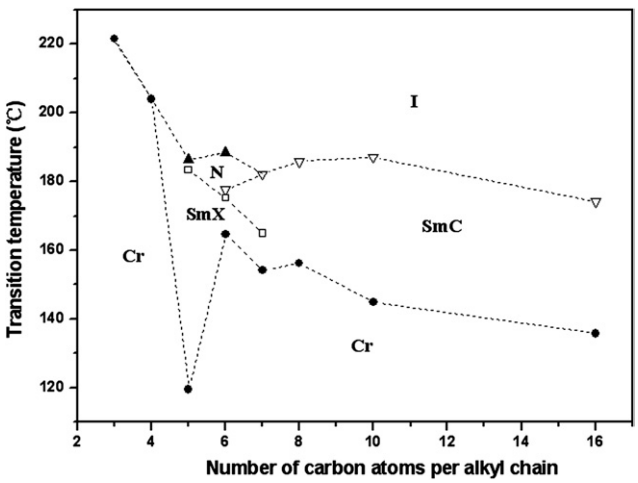

Fig. 5 A plot of the transition temperatures as a function of the length of the terminal *n*-alkyl chain for BOXD-*n* ($n = 3, 4, 5, 6, 7, 8, 10, 16$) on the cooling runs.

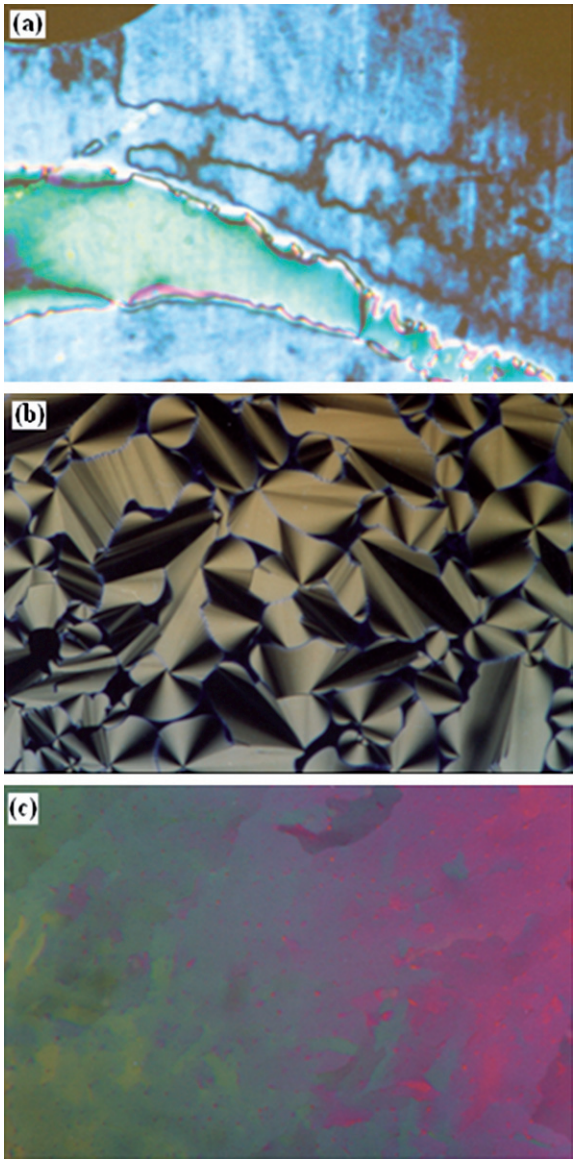

Fig. 6 Optical textures of BOXD-6 (a) at 180 °C (×200); (b) 176 °C (×200), (c) 168 °C (×200) and sandwiched between untreated glass slides.

On further cooling from the nematic phase of BOXD-6, smooth fan-shaped (Fig. 6b) as well as *schlieren* textures were observed, suggesting a smectic phase. The XRD profile of BOXD-6 in Fig. 7b consists of a sharp strong diffraction (20.4 Å) and a weak second order diffraction (10.1 Å) in the small angle regions as well as a diffuse halo centered at 4.5 Å, suggesting a layer structure without in-plane order. The calculated layer spacing from XRD was much smaller than the length of the full extended molecular length, indicating a SmC structure. Interestingly, circular domains were also observed in this SmC phase. Generally, in these domains the smectic layers are circularly arranged around the center of the domains and the direction of dark extinction brushes corresponds to the direction of the optical axes of the smectic layers. In our case, the dark extinction brushes are inclined with the position of polarizer and analyzer indicating the synclinic feature of the SmC phase. Similar textures were also observed in the SmC phases of BOXD-*n*

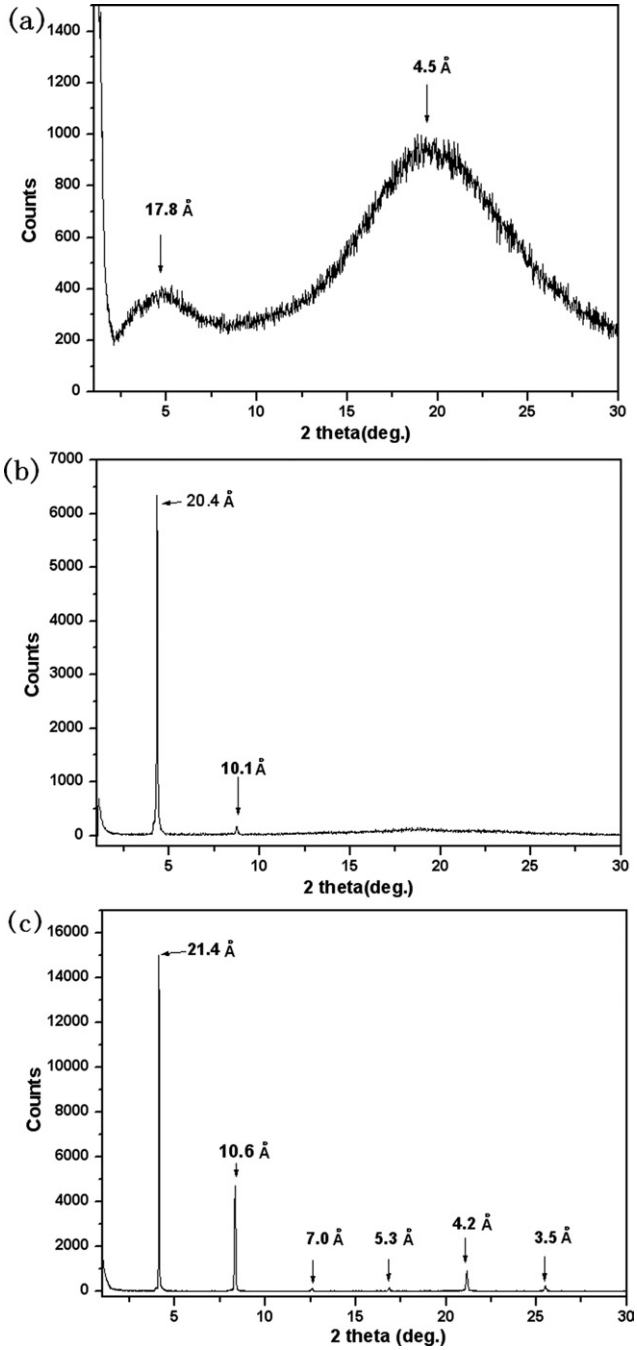

Fig. 7 Powder X-ray diffraction patterns of BOXD-6 (a) at 180 °C; (b) 176 °C and (c) 168 °C.

($n = 7, 8, 10, 16$) on cooling from the isotropic state (Fig. 8). The layer spacing values (d) in SmC of BOXD-n ($n = 6, 7, 8, 10, 16$) collected in Table 2, showed temperature-independence and as an example, a plot of the layer spacing values (d) in the SmC phase of BOXD-10 as a function temperature is shown in Fig. 9. The ratios of the layer spacing value (d) and the geometry optimized molecular length assuming a fully extended alkyl tails (l) in the SmC phases of BOXD-n ($n = 6, 7, 8, 10, 16$) are in the range of 0.62 to 0.64, suggesting BOXD-n molecules are large angle tilted (about 50°) from the layer normal, which was relatively rare in other reported SmC phases. Compared to that of the

Table 2 Summary of the X-ray diffraction results of BOXD-*n* ($n = 6, 7, 8, 10, 16$) in their SmC phases

Compound	Molecular length (l)/Å	T/°C	Layer spacing (d)/Å	d/l	Calculated tilting angle/°
BOXD-6	32.4	176	20.4	0.63	51
BOXD-7	34.5	180	22.0	0.64	50
BOXD-8	36.1	185	22.8	0.63	51
BOXD-10	40.4	163	25.8	0.64	50
BOXD-16	56.9	170	35.1	0.62	52

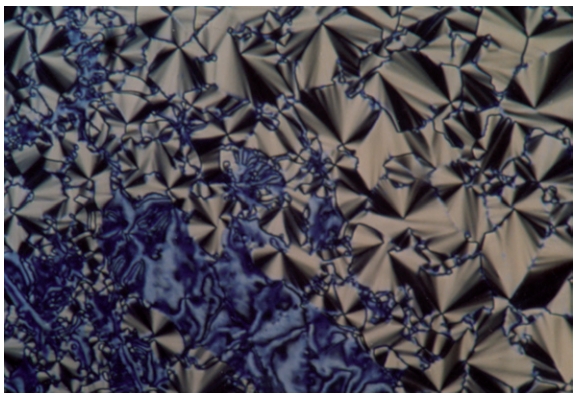

Fig. 8 Optical textures of BOXD-10 at 165 °C (×200) showing regions of fans co-existing with a schlieren texture (sample sandwiched between untreated glass slides).

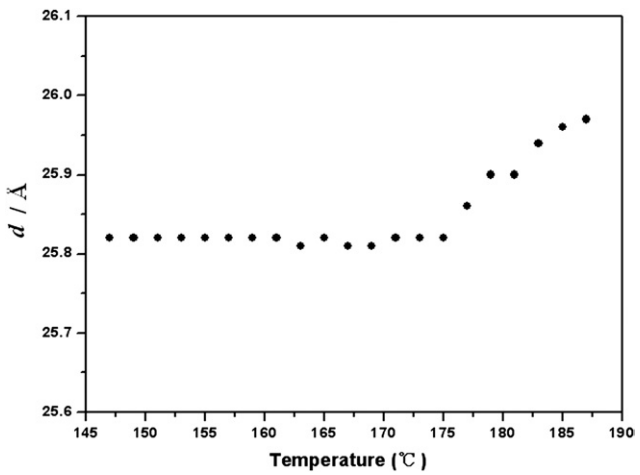

Fig. 9 The layer spacing value (d) as a function of temperature in the SmC phase of BOXD-10 on the cooling runs.

conventional smectic–isotropic transition (1–10 kJ mol^{-1}), BOXD-*n* ($n = 7, 8, 10, 16$) showed larger enthalpic values (17.1–19.2 kJ mol^{-1}) in the SmC–I transition, suggesting that strong intermolecular interactions remained in these SmC phases.

On further cooling from the SmC phase of BOXD-6 and BOXD-7, a high ordered smectic phase developed within which relatively large domains with uniform colors (Fig. 6c) were observed. The highly ordered layer structure in this mesophase of BOXD-6 was confirmed by X-ray diffraction, which showed a sharp strong diffraction (21.4 Å) and up to sixth order diffractions, indicating its well-defined layer structure with sharp interfaces (Fig. 7c). At this stage, however, we do not have sufficient experimental evidence to identify this smectic phase. Thus, we denote this phase the SmX phase hereafter. The SmX phase was also observed in BOXD-5 upon cooling from its nematic phase.

Interestingly, relatively large scale monodomains of BOXD-5 with uniform colors developed by slowly cooling down the nematic phase to the SmX phase even without any surface treatment. For illustration, Fig. 10 showed that domains A and B in the SmX phase of BOXD-5 exhibit alternate changes in uniform brightness and darkness by rotating the sample stage, suggesting the characteristics of the monodomain.

It should be noted that the ratios of the layer spacing value (d) and the geometry optimized molecular length assuming fully extended alkyl tails (l) in the SmC phases of BOXD-*n* ($n = 6, 7, 8,$

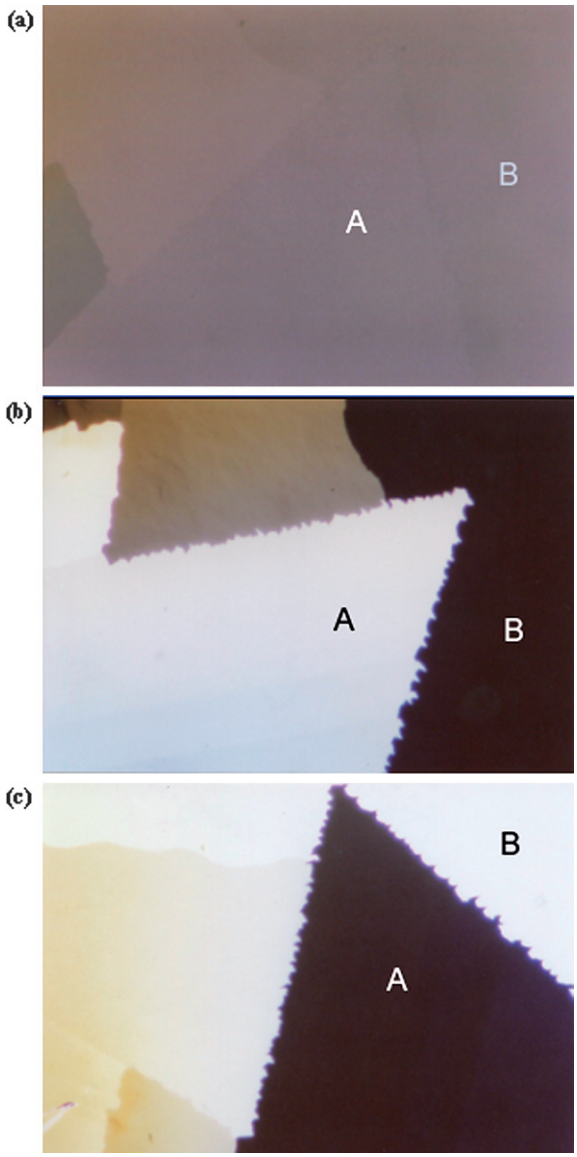

Fig. 10 Optical textures for the SmX phase of BOXD-5 at 150 °C (×100). A and B domains were observed by rotating the sample stage of (a) 0°, (b) −30° and (c) 30° under crossed polarizers (the sample was sandwiched between untreated glass slides).

10, 16) remained almost unchanged (in the range of 0.62 to 0.64), although the aliphatic tails increased, indicating that peculiar intermolecular interaction between adjacent rigid segments is responsible for the peculiar mesogenic behavior of BOXD-*n*. It is reasonable that the rigid segment of BOXD-*n* is regarded as a D–A–A–D array. Compared to the SmA-like packing model with mesogens parallel to each other and perpendicular to the layer normal, the SmC-like arrangement will be the most probable packing mode, because slipping of such D–A–A–D arrays with each other will lead oxadiazole rings [acceptor (A) groups] to be close to phenyl rings [donor (D) groups], and thus cause intermolecular donor–acceptor interactions, which were thought to be the driving force for the BOXD-*n* molecules large angle tilting in layers observed both in single-crystals of BOXD-1 and 2D arrangement of BOXD-7 and BOXD-16 on HOPG. We propose that intermolecular electron donor–acceptor interactions between oxadiazole rings and phenyl rings are responsible for the peculiar smectic structureof BOXD-*n*. The proposed packing model of BOXD-*n* in the smectic C phases is shown in Scheme 2. In this model, BOXD-*n* molecules tilted with a large angle to the layer normal, *e.g.* oxadiazole rings [acceptor (A) groups] are close to the neighboring phenyl rings [donor (D) groups] due to the intermolecular donor–acceptor interactions and thus stabilize the mesophases. The proposed model of BOXD-*n* in the smectic C phases was supported by the following experimental evidence: (1) the molecules tilt against the layer normal with an angle of about 50°, which is similar to that observed in X-ray single-crystal diffraction of BOXD-1 and the STM images of BOXD-7 and BOXD-16 on HOPG; (2) temperature-independent *d*-spacing in the range of SmC phases; (3) larger enthalpic changes of SmC-I transition in BOXD-*n* compared to that of the conventional calamitic mesogens. Considering the larger enthalpy values on transition from the nematic to the isotropic phase of BOXD-5 and BOXD-6, we suggest that the intermolecular electron donor–acceptor interaction still exists in the nematic phase, although it might be weaker than that in the crystalline or in the smectic phase due to the increased freedom of molecules at higher temperatures. The enthalpy values on transition from nematic to SmX phase of BOXD-5 is up to 25.7 kJ mol^{-1}, indicating that the intermolecular donor–acceptor interactions were strong enough to sustain long-range ordering and thus to form relatively large scale monodomains developed from the lower ordered nematic phase.

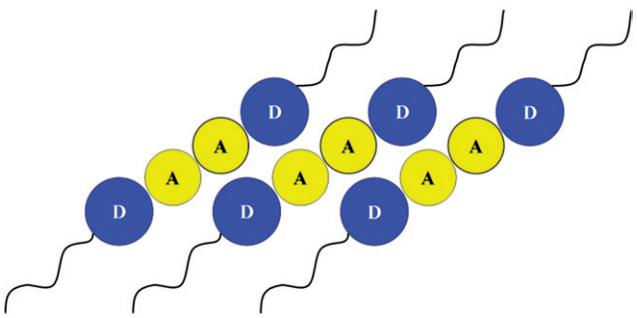

Scheme 2 Schematic representation of BOXD-*n* molecules packing in the tilted smectic C phase, illustrating the supramolecular stacks consisting of alternating donor and acceptor along the stack axis, resulting in the large angle tilting within the smectic layers; the blue parts D correspond to phenyl rings (donor groups) and the yellow parts A correspond to oxadiazole rings (acceptor groups).

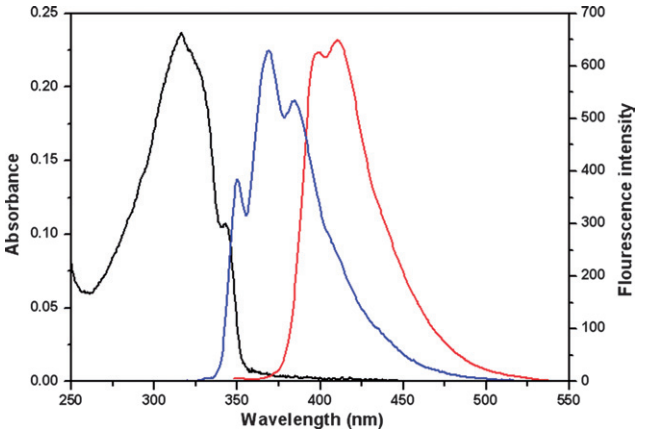

Fig. 11 UV-vis (black line) and PL spectra of BOXD-6 in cyclohexane (1×10^{-5}mol L^{-1}) (blue line) and solid state (red line) at room temperature.

Optical properties

The UV-vis absorption and photoluminescence spectra for BOXD-6 in cyclohexane are presented in Fig. 11. The photophysical properties of BOXD-*n* in cyclohexane (1×10^{-5} mol L^{-1}) are summarized in Table S1.† The absorption spectra of BOXD-*n*, in which an intense broad absorption at 316 nm was observed, were similar in shape because of their structural similarities. The PL spectra of BOXD-*n* were recorded in cyclohexane at $\lambda_{exc.}$ = 330 nm. All the compounds exhibit strong emission fluorescence with three maxima at 350, 368 and 384 nm. Fluorescence quantum yields were determined relative to a solution of quinine bisulfate in 0.1 N H_2SO_4 ($\Phi_F = 0.515$) and calculated according to the literature.[24] All the compounds exhibited high quantum yields ($\Phi_F > 90\%$) in cyclohexane (1×10^{-5} mol L^{-1}).

In addition, all BOXD-*n* exhibited strong emission fluorescence in the solid state. For example, BOXD-6 in the solid state (crystallized from DMSO) shows strong fluorescence in the blue spectral region ($\lambda_{max.}$ = 398, 410 nm) with an efficiency Φ_F of up to 57% (Φ_F in the solid state is obtained in a calibrated integrating sphere),[25] as shown in Fig. 9.

Conclusions

A new series of bi-1,3,4-oxadiazole derivatives [2,2′-bis(4-alkoyphenyl)-bis-1,3,4-oxadiazole, BOXD-*n*, *n* = 1, 3, 4, 5, 6, 7, 10, 16] were designed and synthesized. Fully conjugated conformations were demonstrated either by computer simulation or in the single-crystal state. Well-defined 3D DA architectures with strong face-to-face and edge-to-edge donor–acceptor interactions were observed in the single =-crystal structure of BOXD-1. Nematic phase, SmC phase with a large tilt angle ($\theta \approx 50°$) and relatively large transition enthalpic values and a highly ordered SmX phase were demonstrated in BOXD-*n* (*n* = 5, 6, 7, 8, 10, 16) through tailing the terminal chains and relatively large scale monodomains were prepared in the SmX phase of BOXD-5 even without any surface treatment. Strong blue fluorescent emissions were observed in BOXD-6 either in cyclohexane

($\Phi_F \approx 92\%$) or in the solid state ($\Phi_F \approx 57\%$). The strong donor–acceptor interaction between the alkyoxyphenylene ring and the 1,3,4-oxadiazole ring was thought to be the driving force for the molecules to self-assemble into large angle tilted layered structure. The present work revealed that BOXD-*n* could be used as an ideal model compound for building DA architectures, such as supramolecular sheets, stacks or even 3D arrays. Potential applications for these compounds, such as optoelectronic applications or even non-linear optical generation properties, are of interest and will be investigated further.

Experimental

General methods

Ethyl *p*-hydroxybenzoate,oxalyl chloride, and 1-bromide alkane were used as received. 4-Alkoxy-benzoyl hydrazine **2** was prepared according to the literature.[26] Tetrahydrofuran (THF) was refluxed over sodium under argon and distilled before use. Oxalyl chloride (11 mmol) was regularly injected into the THF solution of 4-alkoxy-benzoyl hydrazine **2** (23 mmol) with vigorous stirring at room temperature for 8 h, yielding the products oxalyl acid *N*′,*N*′-di(4-alkoxylbenzoyl)-hydrazide **3**, which were purified by washing with alcohol.

Characterization

^{1}H NMR spectra were recorded with a Bruker Avance 500 MHz or a Varian-300 EX spectrometer, using $CDCl_3$ as a solvent and tetramethylsilane (TMS) as an internal standard ($\delta = 0.00$ ppm). ^{13}C NMR spectra were recorded with a Varian-300 EX spectrometer, using $CDCl_3$ as a solvent and $CDCl_3$ as an internal standard ($\delta = 77.00$ ppm). FT-IR spectra were recorded with a Perkin–Elmer spectrometer (Spectrum One B). The samples were pressed tablets with KBr. Phase transitional properties were investigated by differential scanning calorimeter (DSC, Mettler Star DSC 821^e). Optical textures were observed under a polarized optical microscope (POM, Leica DMLP) equipped with a Leitz 350 heating stage. X-Ray diffraction (XRD) was carried out with a Bruker Avance D8 X-ray diffractometer. STM measurements were carried out with a Nano IIIa Multimode SPM (Digital Instruments, Santa Barbara, USA). The molecules were dissolved in 1-phenylocatane (98%, Aldrich) at a concentration of about 1 mg mL^{-1}. Then a small droplet (~3 μL) of such a solution was deposited onto a freshly cleaved HOPG (NT-MDT, ZYB grade) substrate. STM imaging was performed by using a mechanically cut Pt/Ir tip (80 : 20, 0.25 mm in diameter) and scanned at the solution–HOPG interface. All STM images presented here were flattened and low pass-filtered without any further treatments.

Oxalyl acid *N*′,*N*′-di(4-propyloxybenzoyl)-hydrazide

^{1}H NMR: (300 MHz, *d*6-DMSO), (ppm, from TMS): 10.75 (s, 2 H); 10.35 (s, 2 H); 7.87 (d, 4 H, $J = 8.8$ Hz); 7.05 (d, 4 H, $J = 8.8$ Hz); 4.01 (t, 4 H, $J = 6.5$ Hz); 1.78–1.71 (m, 4 H); 0.99 (t, 6 H, $J = 7.2$ Hz); FT-IR (KBr disc, cm^{-1}): 3428, 3205, 2966, 2939, 2879, 1691, 1648, 1609, 1567, 1508, 1441, 1418, 1394, 1342, 1307, 1257, 1180, 1144, 1117, 1068, 1016, 977, 906, 846, 824, 759, 691, 649, 627; anal. calcd for $C_{22}H_{26}N_4O_6$: C, 59.72; H, 5.92; N, 12.66. Found C, 59.64; H, 6.17; N, 12.69.

Oxalyl acid *N*′,*N*′-di(4-heptyloxybenzoyl)-hydrazide

^{1}H NMR: (500 MHz, *d*6-DMSO), (ppm, from TMS): 10.72 (s, 2 H); 10.33 (s, 2 H); 7.86 (d, 4 H, $J = 8.8$ Hz); 7.03 (d, 4 H, $J = 8.8$ Hz); 4.04 (t, 4 H, $J = 6.5$ Hz); 1.76–1.70 (m, 4 H); 1.45–1.39 (m, 4 H); 1.36–1.27 (m, 12 H); 0.87 (t, 6 H, $J = 6.8$ Hz); FT-IR (KBr disc, cm^{-1}): 3191, 2955, 2939, 2927, 2861, 1689, 1646, 1608, 1578, 1508, 1475, 1465, 1417, 1393, 1342, 1307, 1253, 1179, 1119, 1039, 1014, 989, 907, 850, 824, 730, 689, 652, 630; anal. calcd for $C_{30}H_{42}N_4O_6$: C, 64.96; H, 7.63; N, 10.10. Found C, 64.67; H, 7.87; N, 10.09.

Oxalyl acid *N*′,*N*′-di(4-octyloxybenzoyl)-hydrazide

^{1}H NMR: (300 MHz, *d*6-DMSO), (ppm, from TMS): 10.76 (s, 2 H); 10.35 (s, 2 H); 7.86 (d, 4 H, $J = 8.8$ Hz); 7.04 (d, 4 H, $J = 8.8$ Hz); 4.04 (t, 4 H, $J = 6.5$ Hz); 1.76–1.70 (m, 4 H); 1.45–1.27 (m, 20 H); 0.87 (t, 6 H, $J = 6.8$ Hz); FT-IR (KBr disc, cm^{-1}): 3215, 2953, 2926, 2854, 1697, 1647, 1612, 1570, 1512, 1467, 1439, 1414, 1396, 1309, 1282, 1255, 1176, 1146, 1116, 1044, 1027, 999, 968, 908, 845, 781, 760, 703, 650; anal. calcd for $C_{32}H_{46}N_4O_6$: C, 65.96; H, 7.96; N, 9.61. Found C, 66.26; H, 7.93; N, 9.82.

Oxalyl acid *N*′,*N*′-di(4-decyloxybenzoyl)-hydrazide

^{1}H NMR: (300 MHz, *d*6-DMSO), (ppm, from TMS): 10.74 (s, 2 H); 10.34 (s, 2 H); 7.86 (d, 4 H, $J = 8.6$ Hz); 7.04 (d, 4 H, $J = 8.6$ Hz); 4.04 (t, 4 H, $J = 6.5$ Hz); 1.75–1.70 (m, 4 H); 1.44–1.26 (m, 28 H); 0.86 (t, 6 H, $J = 6.8$ Hz); FT-IR (KBr disc, cm^{-1}): 3201, 2956, 2938, 2921, 2852, 1689, 1647, 1608, 1577, 1508, 1474, 1442, 1416, 1393, 1343, 1307, 1255, 1179, 1118, 1050, 1019, 906, 846, 825, 758, 729, 721, 689, 652, 630; anal. calcd for $C_{36}H_{54}N_4O_6$: C, 67.68; H, 8.52; N, 8.77. Found C, 67.57; H, 8.54; N, 8.86.

Oxalyl acid *N*′,*N*′-di(4-cetyloxybenzoyl)-hydrazide

^{1}H NMR: (500 MHz, *d*6-DMSO), (ppm, from TMS): 10.74 (s, 2 H); 10.34 (s, 2 H); 7.86 (d, 4 H, $J = 8.5$ Hz); 7.03 (d, 4 H, $J = 8.7$ Hz); 4.04 (t, 4 H, $J = 6.5$ Hz); 1.75–1.70 (m, 4 H); 1.44–1.38 (m, 4 H); 1.34–1.24 (m, 48 H); 0.85 (t, 6 H, $J = 6.8$ Hz); FT-IR (KBr disc, cm^{-1}): 3229, 2955, 2920, 2850, 1714, 1658, 1612, 1574, 1512, 1471, 1439, 1414, 1399, 1311, 1287, 1255, 1178, 1145, 1116, 1047, 1025, 922, 842, 825, 816, 779, 759, 719, 702, 646, 617; anal. calcd for $C_{48}H_{78}N_4O_6$: C, 71.43; H,9.74; N, 6.94. Found C, 71.29; H, 9.98; N, 6.94.

2,2-Bis(4-propyloxyphenyl)-bi-1,3,4-oxadiazole

^{1}H NMR: (300 MHz, $CDCl_3$), (ppm, from TMS): 8.16 (d, 4 H, $J = 8.9$ Hz); 7.05 (d, 4 H, $J = 8.9$ Hz); 4.03 (t, 4 H, $J = 6.6$ Hz); 1.90–1.83 (m, 4 H); 1.08 (t, 6 H, $J = 7.2$ Hz); FT-IR (KBr disc, cm^{-1}): 2973, 2942, 2885, 2877, 1608, 1581, 1493, 1471, 1425, 1398, 1337, 1338, 1309, 1289, 1268, 1182, 1155, 1126, 1088, 1041, 1010, 951, 910, 901, 839, 815, 768, 741, 702, 671, 656, 630; anal. calcd for $C_{22}H_{22}N_4O_4$: C, 65.01; H, 5.46; N, 13.78. Found C, 65.01; H, 5.57; N, 13.78.

2,2-Bis(4-butyloxyphenyl)-bi-1,3,4-oxadiazole

^{1}H NMR: (300 MHz, $CDCl_3$), (ppm, from TMS): 8.15 (d, 4 H, J = 9.0 Hz); 7.05 (d, 4 H, J = 8.9 Hz); 4.07 (t, 4 H, J = 6.6 Hz); 1.82–1.78 (m, 4 H); 1.59–1.49 (m, 4 H); 1.00 (t, 6 H, J = 7.2 Hz); FT-IR (KBr disc, cm^{-1}): 2960, 2932, 2870, 1608, 1582, 1551,1493, 1470, 1424, 1336, 1308, 1288, 1272, 1256,1177, 1152, 1123, 1112,1082, 1066, 1032,1008, 1001,968, 950,910, 845, 820, 803,741, 702, 668, 653, 630; anal. calcd for $C_{24}H_{26}N_4O_4$: C, 66.34; H, 6.03; N, 12.89. Found C, 66.13; H, 6.12; N, 13.25.

2,2-Bis(4-pentyloxyphenyl)-bi-1,3,4-oxadiazole

^{1}H NMR: (300 MHz, $CDCl_3$), (ppm, from TMS): 8.15 (d, 4 H, J = 9.0 Hz); 7.05 (d, 4 H, J = 8.9 Hz); 4.06 (t, 4 H, J = 6.6 Hz); 1.86–1.79 (m, 4 H); 1.50–1.40 (m, 8 H); 0.95 (t, 6 H, J = 6.9 Hz); FT-IR (KBr disc, cm^{-1}): 2948, 2921, 2870, 1608, 1582, 1493, 1476, 1462,1424, 1395, 1375,1344, 1334, 1307, 1289, 1262,1244, 1182, 1175, 1151, 1122, 1086, 1056, 1004, 951, 901, 837, 809, 741, 726, 701, 655, 630; anal. calcd for $C_{26}H_{30}N_4O_4$: C, 67.51; H, 6.54; N, 12.11. Found C, 67.28; H, 6.58; N, 12.23.

2,2-Bis(4-hexyloxyphenyl)-bi-1,3,4-oxadiazole

^{1}H NMR: (300 MHz, $CDCl_3$), (ppm, from TMS): 8.15 (d, 4 H, J = 8.9 Hz); 7.04 (d, 4 H, J = 8.9 Hz); 4.05 (t, 4 H, J = 6.6 Hz); 1.86–1.78 (m, 4 H); 1.50–1.44 (m, 4 H); 1.38–1.35 (m, 8 H); 0.93 (t, 6 H, J = 6.9 Hz); FT-IR (KBr disc, cm^{-1}): 2951, 2936, 2922, 2868, 2854, 1607, 1581, 1551, 1493, 1473, 1421, 1401, 1389, 1336, 1308, 1291, 1254, 1174, 1153, 1123, 1083, 1058, 1032, 1010, 950, 846, 819,806, 740, 702, 655, 630; anal. calcd for $C_{28}H_{34}N_4O_4$: C, 68.55; H, 6.99; N, 11.42. Found C, 68.31; H, 6.88; N, 11.25.

2,2-Bis(4-heptyloxyphenyl)-bi-1,3,4-oxadiazole

^{1}H NMR: (500 MHz, $CDCl_3$), (ppm, from TMS): 8.17 (d, 4 H, J = 8.9 Hz); 7.06 (d, 4 H, J = 8.9 Hz); 4.07 (t, 4 H, J = 6.6 Hz); 1.86–1.83 (m, 4 H); 1.52–1.49 (m, 4 H); 1.41–1.32 (m, 12 H); 0.92 (t, 6 H, J = 6.9 Hz). ^{13}C NMR (300 MHz, $CDCl_3$): δ = 166.4, 163.1, 152.8, 129.8, 129.6, 115.4, 115.3, 68.7, 68.6, 32.0, 29.3, 26.2, 22.8, 14.3; FT-IR (KBr disc, cm^{-1}): 2927, 2869, 2854, 1607, 1581, 1552, 1493, 1472, 1421, 1391, 1336, 1308, 1290, 1255, 1177, 1152, 1122, 1082, 1034, 1011, 951, 874, 816, 741, 728, 702, 656, 632; anal. calcd for $C_{30}H_{38}N_4O_4$: C, 69.47; H, 7.38; N, 10.80. Found C, 69.57; H, 7.47; N, 10.77.

2,2-Bis(4-octyloxyphenyl)-bi-1,3,4-oxadiazole

^{1}H NMR: (300 MHz, $CDCl_3$), (ppm, from TMS): 8.15 (d, 4 H, J = 8.9 Hz); 7.05 (d, 4 H, J = 8.9 Hz); 4.05 (t, 4 H, J = 6.6 Hz); 1.86–1.79 (m, 4 H); 1.49–1.45 (m, 4 H); 1.35–1.30 (m, 16 H); 0.90 (t, 6 H, J = 6.9 Hz); FT-IR (KBr disc, cm^{-1}): 2950, 2935, 2921, 2854, 1606, 1581, 1493, 1479, 1421, 1400, 1386, 1336, 1307, 1290, 1254, 1174, 1151, 1122, 1081, 1022, 1010, 998, 951, 845, 816, 741, 726, 702, 670, 656, 631; anal. calcd for $C_{32}H_{42}N_4O_4$: C, 70.30; H, 7.74; N, 10.25. Found C, 70.38; H,7.85; N, 10.17.

2,2-Bis(4-decyloxyphenyl)-bi-1,3,4-oxadiazole

^{1}H NMR: (300 MHz, $CDCl_3$), (ppm, from TMS): 8.16 (d, 4 H, J = 8.8 Hz); 7.05 (d, 4 H, J = 8.8 Hz); 4.06 (t, 4 H, J = 6.6 Hz); 1.86–1.80 (m, 4 H); 1.50–1.46 (m, 4 H); 1.35–1.29 (m, 24 H); 0.89 (t, 6 H, J = 6.9 Hz); FT-IR (KBr disc, cm^{-1}): 2952, 2922, 2852, 1606, 1581, 1555, 1493, 1473, 1422, 1401, 1336, 1308, 1292, 1257, 1174, 1154, 1122, 1081, 1048, 1016, 996, 951, 845, 818, 741, 723, 703, 656, 632; anal. calcd for $C_{36}H_{50}N_4O_4$: C, 71.73; H, 8.36; N, 9.29. Found C, 71.85; H, 8.68; N, 9.35.

2,2-Bis(4-cetyloxyphenyl)-bi-1,3,4-oxadiazole

^{1}H NMR: (300 MHz, $CDCl_3$), (ppm, from TMS): 8.16 (d, 4 H, J = 8.8 Hz); 7.05 (d, 4 H, J = 8.8 Hz); 4.06 (t, 4 H, J = 6.6 Hz); 1.86–1.80 (m, 4 H); 1.50–1.46 (m, 4 H); 1.35–1.26 (m, 48H); 0.88 (t, 6 H, J = 6.9 Hz); FT-IR (KBr disc, cm^{-1}): 2954, 2920, 2850, 1606, 1851, 1553, 1493, 1473, 1423, 1399, 1388, 1335, 1308, 1293, 1256, 1180, 1173, 1153, 1121, 1081, 1044, 1019, 999, 974, 951, 847, 815, 740, 722, 702, 657, 632; anal. calcd for $C_{48}H_{74}N_4O_4$: C, 74.76; H, 9.67; N, 7.27. Found C, 74.79; H, 9.89; N, 7.40.

Acknowledgements

The authors are grateful to the National Science Foundation Committee of China (project no. 50373016 and 20433010), Program for New Century Excellent Talents in Universities of China Ministry of Education, Special Foundation for PhD Programmes in Universities of China Ministry of Education (Project No. 20050183057), and Project 985-Automotive Engineering of Jilin University for their financial support of this work.

References

1 (*a*) Special issue on Supramolecular Chemistry & Self-Assembly, *Science*, 2002, **295**, 2313–2556; (*b*) T. Kato, *Science*, 2002, **295**, 2414–2418; (*c*) J. T. Davis, *Angew. Chem.*, 2004, **116**, 684–716; J. T. Davis, *Angew. Chem., Int. Ed.*, 2004, **43**, 668–698; (*d*) G. Gottarelli, G. P. Spada and A. Garbesi, in *Comprehensive Supramolecular Chemistry*, ed. J.-M. Lehn, J. L. Atwood, J. E. D. Davies, D. D. MacNicol, F. Vötle, J.-P. Sauvage and M. W. Hosseini, Pergamon, Oxford, 1996, vol. 5, pp. 483–506; (*e*) G. Gottarelli and G. P. Spada, *Chem. Rev.*, 2004, **4**, 39–49; (*f*) L. Brunsveld, B. J. B. Folmer, E. W. Meijer and R. P. Sijbesma, *Chem. Rev.*, 2001, **101**, 4071–4097; (*g*) M. Muthukumar, C. K. Ober and E. L. Thomas, *Science*, 1997, **277**, 1225–1232; (*h*) S. I. Stupp, V. LeBonheur, K. Walker, L. S. Li, K. E. Huggins, M. Keser and A. Amstutz, *Science*, 1997, **276**, 384–389.

2 (*a*) G. R. Desiraju, *Crystal Engineering*, Elsevier, Amsterdam, 1989; (*b*) H. Bock, W. Seitz, M. Sievert, M. Kleine and J. W. Bats, *Angew. Chem., Int. Ed. Engl.*, 1996, **35**, 2244–2246; (*c*) M. L. Greer, J. R. Duncan, J. L. Duff and S. C. Blackstock, *Tetrahedron Lett.*, 1997, **38**, 7665–7668; (*d*) B. Colonna, S. Menzer, F. M. Raymo, J. F. Stoddart and D. J. Williams, *Tetrahedron Lett.*, 1998, **39**, 5155–5158; (*e*) E. Bosch, S. M. Hubig, S. V. Lindeman and J. K. Kochi, *J. Org. Chem.*, 1998, **63**, 592; (*f*) G. W. Coates, A. R. Dunn, L. M. Henling, J. W. Ziller, E. B. Lobokovsky and R. H. Grubbs, *J. Am. Chem. Soc.*, 1998, **120**, 3641; (*g*) E. Bosch, R. Radford and C. L. Barnes, *Org. Lett.*, 2001, **3**, 881–883.

3 (*a*) R. Rathore, S. V. Lindeman and J. K. Kochi, *J. Am. Chem. Soc.*, 1997, **119**, 9393; (*b*) D. G. Hamilton, J. E. Davies, L. Prodi and J. K. M. Sanders, *Chem.–Eur. J.*, 1998, **4**, 608–620; (*c*) A. C. Try, M. M. Harding, D. G. Hamilton and J. K. M. Sanders, *Chem. Commun.*, 1998, 723–724; (*d*) D. G. Hamilton and J. K. M. Sanders, *Chem. Commun.*, 1998, 1749–1750; (*e*) D. G. Hamilton, N. Feeder, L. Prodi, S. J. Test, W. Clegg and J. K. M. Sanders, *J. Am. Chem. Soc.*, 1998, **120**, 1096–1097; (*f*) D. G. Hamilton, N. Feeder, S. J. Teat and J. K. M. Sanders, *New J. Chem.*, 1998, **22**, 1019–1021; (*g*) D. G. Hamilton, L. Prodi, N. Feeder and J. K. M. Sanders, *J. Chem. Soc., Perkin Trans. 1*,

1999, 1057–1066; (*h*) D. G. Hamilton, M. Montalti, L. Prodi, M. Fontai, P. Zanello and J. K. M. Sanders, *Chem.–Eur. J.*, 2000, **6**, 608–617; (*i*) J. G. Hansen, N. Feeder, D. G. Hamilton, M. J. Gunter, J. Becher and J. K. M. Sanders, *Org. Lett.*, 2000, **2**, 449–452; (*j*) M. J. Gunter, N. Bampos, K. D. Johnstone and J. K. M. Sanders, *New J. Chem.*, 2001, **25**, 166–173; (*k*) K. D. Johnstone, N. Bampos, J. K. M. Sanders and M. J. Gunter, *Chem. Commun.*, 2003, 1396–1397; (*l*) T. Iijima, S. A. Vignon, H. R. Tseng, T. Jarrosson, J. K. M. Sanders, F. Marchioni, M. Venturi, E. Apostoli, V. Balzani and J. F. Stoddart, *Chem.–Eur. J.*, 2004, **10**, 6375–6392.

4 (*a*) R. M. Metzger, *Acc. Chem. Res.*, 1999, **32**, 950–957; (*b*) W. B. Davis, W. A. Svec, M. A. Ratner and M. R. Wasielewski, *Nature*, 1998, **396**, 60–63; (*c*) C. Joachim, J. K. Gimzewski and A. Aviram, *Nature*, 2000, **408**, 541–548; (*d*) F. J. M. Hoeben, P. Jonkheijm, E. W. Meijer and A. P. H. J. Schenning, *Chem. Rev.*, 2005, **105**, 1491–1546.

5 (*a*) M. O'Neill and S. M. Kelly, *Adv. Mater.*, 2003, **15**, 1135; (*b*) A. J. J. M. van Breemen, P. T. Herwig, C. H. T. Chlon, J. Sweelssen, H. F. M. Schoo, S. Setayesh, W. M. Hardeman, C. A. Martin, D. M. de Leeuw, J. J. P. Valeton, C. W. M. Bastiaansen, D. J. Broer, A. R. Popa-Merticaru and S. C. J. Meskers, *J. Am. Chem. Soc.*, 2006, **128**, 2336.

6 (*a*) J. W. Park, C. S. Bak and M. M. Labes, *J. Am. Chem. Soc.*, 1975, **97**, 4398; (*b*) R. Deschenaux, M. Schweissguth and A.-M. Levelut, *Chem. Commun.*, 1996, 1275; (*c*) H. Bengs, M. Ebert, O. Karthaus, B. Kohne, K. Praefcke, H. Ringsdorf, J. H. Wendorff and R. Wustefeld, *Adv. Mater.*, 1990, **2**, 141–144; (*d*) W. Pisula, M. Kastler, D. Wasserfallen, J. W. F. Robertson, F. Nolde, C. Kohl and K. Müllen, *Adv. Mater.*, 2006, **45**, 819–823; (*e*) K. Praefcke and D. Singer, in *Handbook of Liquid Crystals*, eds. D. Demus, J. Goodby, G. W. Gray, H.-W. Spiess and V. Vill, Wiley-VCH, Weinheim, 1998, vol. 2B, p. 944.

7 (*a*) W. Kranig, C. Boeffel, H. W. Spiess, O. Karthaus, H. Ringsdorf and R. Wustefeld, *Liq. Cryst.*, 1990, **8**, 375; (*b*) V. V. Tsukruk, J. H. Wendorff, O. Karthaus and H. Ringsdorf, *Langmuir*, 1993, **9**, 614.

8 (*a*) N. Boden, R. J. Bushby, Z. B. Lu and O. R. Lozman, *Liq. Cryst.*, 2001, **28**, 657; (*b*) E. O. Arikainen, N. Boden, R. J. Bushby, O. R. Lozman, J. G. Vinter and A. Wood, *Angew. Chem.*, 2000, **112**, 2423; (*c*) E. O. Arikainen, N. Boden, R. J. Bushby, O. R. Lozman, J. G. Vinter and A. Wood, *Angew. Chem., Int. Ed.*, 2000, **39**, 2333.

9 L. Y. Park, D. G. Hamilton, E. A. McGehee and K. A. McMenimen, *J. Am. Chem. Soc.*, 2003, **125**, 10586.

10 (*a*) B. R. Wegewijs, L. D. A. Siebbeles, N. Boden, R. J. Bushby, B. Movaghar, O. R. Lozman, Q. Liu, A. Pecchia and L. A. Mason, *Phys. Rev. B*, 2002, 65; (*b*) A. Pecchia, O. R. Lozman, B. Movaghar, N. Boden, R. J. Bushby, K. J. Donovan and T. Kreouzis, *Phys. Rev. B*, 2002, 65; (*c*) T. Kreouzis, K. Scott, K. J. Donovan, N. Boden, R. J. Bushby, O. R. Lozman and Q. Liu, *Chem. Phys.*, 2000, **262**, 489.

11 D. Janietz, *J. Mater. Chem.*, 1998, **8**, 265–274.

12 (*a*) D. Janietz, *Chem. Commun.*, 1996, 713–714; (*b*) D. Goldmann, S. Mahlstedt, D. Janietz, P. Busch, C. Schmidt, A. Stracke and J. H. Wendorff, *Liq. Cryst.*, 1998, **24**, 881–890.

13 (*a*) B. Schultz, M. Bruma and L. Brehmer, *Adv. Mater.*, 1997, **9**, 601; (*b*) M. Thelakkat and H.-W. Schmidt, *Polym. Adv. Technol.*, 1998, **9**, 429; (*c*) G. Hughes and M. R. Bryce, *J. Mater. Chem.*, 2005, **15**, 94–107.

14 B. Schulz, I. Orgzall, A. Freydank and C. Xü, *Adv. Colloid Interface Sci.*, 2005, **116**, 143–164, and references therein.

15 B. G. Kim, S. Kim and S. Y. Park, *Tetrahedron Lett.*, 2001, **42**, 2697.

16 (*a*) C. K. Lai, Y. C. Ke, J. C. Su, C. S. Lu and W. R. Li, *Liq. Cryst.*, 2002, **29**, 915; (*b*) C. R. Wen, Y. J. Wang, H. C. Wang, H. S. Sheu, G. H. Lee and C. K. Lai, *Chem. Mater.*, 2005, **17**, 1646–1654; (*c*) Y. D. Zhang, K. G. Jespersen, M. Kempe, J. A. Kornfield, S. Barlow, B. Kippelen and S. R. Marder, *Langmuir*, 2003, **19**, 6534.

17 H. Tokuhisa, M. Era and T. Tsutsui, *Adv. Mater.*, 1998, **10**, 404.

18 S. Qu and M. Li, *Tetrahedron*, 2007, **63**, 12429.

19 S. Qu, F. Li, H. Wang, B. Bai, C. Xu, L. Zhao, B. Long and M. Li, *Chem. Mater.*, 2007, **19**, 4839.

20 B. König and H. Butenschön, *Memofix Organische Chemie*, Wiley VCH, Weinheim, 2nd edn, 1999.

21 (*a*) S. Fujii, U. Akiba and M. Fujihira, *Chem. Commun.*, 2001, 1688; (*b*) S. Yoshimoto, E. Tsutsumi, Y. Honda, Y. Murata, M. Murata, K. Komatsu, O. Ito and K. Itaya, *Angew. Chem.*, 2004, **116**, 3106; S. Yoshimoto, E. Tsutsumi, Y. Honda, Y. Murata, M. Murata, K. Komatsu, O. Ito and K. Itaya, *Angew. Chem., Int. Ed.*, 2004, **43**, 3044; (*c*) G. B. Pan, J. M. Liu, H. M. Zhang, L. J. Wan, Q. Y. Zheng and C. L. Bai, *Angew. Chem.*, 2003, **115**, 2853; G. B. Pan, J. M. Liu, H. M. Zhang, L. J. Wan, Q. Y. Zheng and C. L. Bai, *Angew. Chem., Int. Ed.*, 2003, **42**, 2747; (*d*) S. De Feyter and F. C. De Schryver, *J. Phys. Chem. B*, 2005, **109**, 4290.

22 D. Rohde, C. J. Yan, H. J. Yan and L. J. Wan, *Angew. Chem., Int. Ed.*, 2006, **45**, 3996–4000, and references therein.

23 (*a*) A. J. Fisher and P. E. Blöchl, *Phys. Rev. Lett.*, 1993, **70**, 3263; (*b*) Z. Mu, X. Yang, Z. Wang, X. Zhang, J. Zhao and Z. Bo, *Langmuir*, 2004, **20**, 8892–8896.

24 K. Q. Ye, J. Wang, H. Sun, Y. Liu, Z. C. Mu, F. Li, S. M. Jiang, J. Y. Zhang, H. X. Zhang, Y. Wang and C. M. Che, *J. Phys. Chem. B*, 2005, **109**, 8008.

25 Y. Kawamura, H. Sasabe and C. Adachi, *Jpn. J. Appl. Phys., Part 1*, 2004, **43**, 7729.

26 J. H. Kim, J. H. Park and H. Lee, *Chem. Mater.*, 2003, **15**, 3414–3416.

